Systematic Study of Interfacial Interactions Between Clays and an Ionomer

Yan Gao,* Namita Roy Choudhury, Naba K. Dutta

Ian Wark Research Institute, University of South Australia, Mawson Lakes Campus, Mawson Lakes, Adelaide, South Australia 5095, Australia

Received 17 May 2009; accepted 8 January 2010
DOI 10.1002/app.32089
Published online 11 May 2010 in Wiley InterScience (www.interscience.wiley.com).

ABSTRACT: To study the interfacial interactions between an ionomer [poly(ethylene-*co*-acrylic acid) neutralized by zinc salts (PI)] and clays, PI–clay nanocomposites were prepared using a solution method. Two types of commercially available montmorillonite clays respectively K10 and KSF were used, and were modified with organic modifiers with chain lengths of 12–18 carbons. The interactions between the PI, clays, and modifiers were evaluated through study of the structure, morphology, and properties of the PI–clay nanocomposites. We found that the modifiers were successfully intercalated into the clay layers (Fourier transform infrared spectroscopy). The clay modified with a long-chain agent showed an exfoliated nature in the nanocomposite. The thermal stability and storage modulus of PI were improved greatly by the addition of the clays, especially when the long-chain modifier was used (thermogravimetric analysis and dynamic mechanical analysis). The differential scanning calorimetry results show that clay layers are inserted into the clusters because of solvent-directed morphological evolution, so the transition of the ionic domains and the crystallinity of PI are changed. The interaction between PI, the modifier, and the silicate layer played an important role in the determination of the properties of the nanocomposites. © 2010 Wiley Periodicals, Inc. J Appl Polym Sci 117: 3395–3405, 2010

Key words: polymer interfaces; ionomers; nanocomposites; organoclay; thermal properties

INTRODUCTION

Organic–inorganic nanocomposites (NCs) are multifunctional materials with a wide range of interesting properties, and they overcome the poor adhesion/interface problems of microcomposites, which stem from the ability to control the nanoarchitecture of materials at a very early stage of preparation.[1–4] Several routes, such as intercalation,[5–8] electrocrystallization,[9] and sol–gel processing,[10,11] can be used to synthesize hybrid materials. Intercalation involves the use of a unique, self-assembling inorganic material, such as clay, to prepare organic–inorganic hybrid composites, which can be used as host lattices for organic materials because of their platy morphology with a high aspect ratio (20–2000).[12–23] Weak dipolar and van der Waals forces exist between the clay layers, which result in galleries.

The dispersion of clay particles in a polymer matrix can result in the formation of two types of NCs: intercalated and exfoliated. Intercalated clay composites have a definite structure formed by the intercalation of polymers into inorganic layered host lattices, and their properties resemble those of the ceramic host. In contrast, exfoliated polymer–clay NCs have low clay contents, with a separation between the galleries and layers that depends on the polymer content of the composite and the properties of the nanoconfined polymer. The properties of the polymer–clay NCs strongly depend on the interactions between the polymer and the clays.[24]

Montmorillonite (MMT) has a strong intercalation ability to accommodate a number of molecules or polymer chains to become compatible with polymers at a molecular level. A clay with an excess negative charge is miscible with a hydrophilic polymer. To render it compatible with hydrophobic polymers, some organic swelling agents have been used to modify its surface characteristics.[25–33] The conformations of the organic swelling agents in the clay interlayer space depend on the chain length and their cation-exchange capacity. Yano et al.[34] reported that ammonium ions with 10–12 carbon atoms were suitable for the modification of MMT dispersed in dimethylacetamide. Increasing the carbon number of the surfactant decreased the hydrophilicity of

Additional Supporting Information may be found in the online version of this article.

**Present address:* Institute of Materials Engineering, Australian Nuclear Science and Technology Organisation, Lucas Heights, New South Wales, Australia.

Correspondence to: N. R. Choudhury (namita.choudhury@unisa.edu.au).

organophilic MMT. Sikdar et al.[24] reported that the structure orientation of MMT in the NCs was affected by the type of the organic swelling agents. The appearance of the organic modifiers influenced the interaction between the polymer and clays. Often, the collapse of the interlayer structure of MMT occurred because of the thermal decomposition of the small organic chain during processing or annealing. During NC preparation, the ionic bonds between the multilayer chains and silicate dissociate, which results in a predominant multilayer arrangement. Under such conditions, the polymer chain cannot diffuse into the interlayer spaces because of the entropic penalty. Thus, it is very important to precisely determine the right process temperature (when no electrostatic dissociation occurs) and to select the polymer for intercalation (intercalation is possible when the polymer interacts strongly with the clay but weakly with the organic cations). The space between the layered silicates increases and becomes more uniform after intercalation because the miscibility between polymer and clay is improved. Many polymers have been used to synthesize polymer–clay NCs, including poly(methyl methacrylate),[35,36] polystyrene,[37] nylon,[38] acrylonitrile butadiene styrene,[25] and poly(ethylene oxide).[39]

Ionomers, a unique class of polymers, contain small amounts of ionic groups (i.e., <15 mol %), which greatly affect their properties, including the modulus, thermal properties, and viscosity. Several ionic groups come close to each other to form a multiplet because of attractive electrostatic interactions, and multiplets aggregate to form clusters; hence, microphase separation exists in such ionomers. Because an ionomer has both hydrophobic (polymer segment) and hydrophilic (ionic cluster) parts, the clay before and after modification exhibits different interactions with the hydrophobic part or ionic part of the ionomer. Clay with a negatively charged surface could well interact electrostatically with the ionomer. This unique feature of ionomers makes them an attractive class of materials for investigating their reactivity/selectivity with unmodified and modified clays by both solution and melt processes. In particular, interaction between inorganic layered materials and such hydrophilic cluster materials can be efficiently used to disperse the layers of MMT on a nanometer level within the cluster of an ionomer. However, reports on ionomer–clay hybrids are scanty.[40–44] In this study, we prepared ionomer–clay (MMT) NCs using clay modified with various swelling agents. The ionomer was poly(ethylene-*co*-acrylic acid) neutralized by zinc salts (PI; Scheme 1). The clays were MMT clays with two sizes (K10 and KSF). The interaction between PI, the clays, and the swelling agents were evaluated with photoacoustic Fourier transform infrared (PA–FTIR) spectroscopy, atomic force microscopy (AFM), small-angle neutron scattering (SANS), wide-angle X-ray diffraction (XRD), thermogravimetric analysis (TGA), modulated differential scanning calorimetry (MDSC), and dynamic mechanical analysis (DMA).

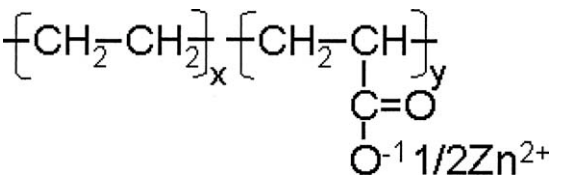

Scheme 1 Chemical structure of PI.

EXPERIMENTAL

Materials

The ionomer was PI (trade name Iotek 4200); it was manufactured by Exxon Chemicals and was received from Qenos Australia. The acrylic acid content in PI was 11 wt %, of which 14 mol % was neutralized. Two kinds of MMT clays (K10 and KSF) were used in our investigation and were purchased from Aldrich. The swelling agents used were dodecyltrimethylammonium bromide (C12), cetyltrimethylammonium bromide (C16), and octadecyltrimethylammonium bromide (C18; Sigma-Aldrich, Sydney). The solvents used were a mixture of toluene and *n*-butanol.

Preparation of the organically modified clay

K10 and KSF were modified with various swelling agents, as reported in our earlier communication.[45] Five grams of clay (K10 or KSF) was dispersed in a solvent (a mixture of toluene and butanol) with stirring. An extra amount of C*x* (where $x = 12$, 16, or 18) was added to the mixture, which was equal to the amount of the clays. The dispersion was stirred at high speed for 1 h at 80°C followed by filtration of the precipitate. MilliQ water was used to wash the precipitate until no white precipitate was observed from the filtrate with silver nitrate; this indicated that the free surfactant was washed away from the modified clay. The white precipitate was AgBr from the reaction between silver nitrate and the surfactants. The modified clay was dried at ambient temperature for 1 week and then placed in an oven for complete drying. The samples are abbreviated as K10–C*x* or KSF–C*x*.

Surface area analysis was done after the clay modification to monitor the progress of modification; for example, the BET surface area of original KSF was 20.95 m^2/g, whereas the BET surface area of KSF–C16 was 8.05 m^2/g. The reduction in the surface

area indicated a covering of the clay surface by C16 chains.

Preparation of the NCs

The NCs reported in this study were prepared via a solution method to prevent any thermal decomposition of the clay's organic treatment. PI was dissolved in the solvent mixture (toluene and butanol) to form a 10 wt % solution. The unmodified/modified clay K10–C*x* or KSF–C*x* was added to this solution with stirring until it became homogeneous. The clay content in the mixture was 10 wt %. The mixture was stirred for 1 h at 80°C, then poured into a Teflon Petri dish to cast a film, and left at room temperature for 2 days; the film was subsequently dried in an oven and then aged for 1 week. The NC samples were slightly yellowish in color and transparent. The yellow color was due to the color of the clay and became lighter after the modification. All of the tests were performed on the film 24 h after sample preparation and were duplicated.

Structural characterization

PA–FTIR spectroscopy was used to study the interaction between the PI, clays, and swelling agents. A Nicolet Magna spectrometer (model 750) (Nicolet Instrument Inc., Madison) equipped with a MTEC (model 300) photoacoustic cell was used. The resolution was 8 cm^{-1}, and the run consisted of 256 scans.

Thermal analysis

TGA measurements were done on duplicate samples with a TA 2995 thermal analyzer (TA Instruments, Delaware) in a nitrogen atmosphere at a flow rate 50 mL/min. The samples were heated from 30 to 600°C at a 10°C/min heating rate. The onset of decomposition, the weight loss, and the residue remaining at 600°C were evaluated.

MDSC was conducted with a DSC 2920 from TA Instrument, Delaware to analyze the melting/crystallization behavior. The sample ($\sim$ 6 mg) was first heated from 30 to 120°C at 20°C/min in the differential scanning calorimetry (DSC) mode; then cooled to 30°C at 0.5, 2, and 5°C/min cooling rates; and finally, heated again from 30 to 120°C at 2°C/min heating rate with an amplitude of modulation of $\pm$0.2°C and a period of 40 s in MDSC mode. The heat flow associated with the transitions in the materials as a function of time and temperature was measured.

Dynamic mechanical properties were measured with a DMA 2980 instrument (TA Instruments). The sample size was 15 $\times$ 2 $\times$ 0.5 mm^3 (Length $\times$ Width $\times$ Thickness). Each measurement was done in duplicate. The module DMA multifrequency tension mode was used with a static force of 1 N and a frequency of 1 Hz. The sample was heated from -150 to 100°C at 3°C/min heating rate.

Morphology characterization

AFM measurements were performed with an Nanoscope IIIa atomic force microscope (Digital Instruments) in the tapping mode. The scan frequency was 1.001 Hz.

A wide-angle XRD experiment was performed at a Difftech MMA X-ray diffractometer with Cu Kα radiation (wavelength = 1.54 Å) The scan was performed from 0 to 30° with a step size of 0.02° and a speed of 3°/min. The crystal morphology of polyethylene (PE) from the NCs was evaluated from the XRD results.

SANS was used to obtain structural information of the clay–polymer NCs. The samples, which were about 1 mm thick, were cyclically exposed to the neutron beam for a total of 4 h (four cycles each 1 h in duration). Neutrons with a wavelength of 3 Å were incident on each sample, and the scattered neutrons were collected on a two-dimensional position-sensitive detector. The collimation length was 5000 mm, and the sample-to-detector distance was also 5000 mm. The neutron beam had a diameter of 10 mm at the sample position and a flux of approximately 2 $\times$ 10^4 neutrons/cm^2/s. The q (q is scattering vector) range was 0.012–0.14 $Å^{-1}$.

RESULTS AND DISCUSSION

Clay modification

The interaction between a polymer and clay depends strongly on the structure and molecular environment of the organic interlayer; therefore, an in-depth understanding of the intercalation process and the formation of organoclay is critical. The degree of substitution generally depends on the structure and reactivity of the clay. This study showed that clay modification was successful for both K10 and KSF [Fourier transform infrared (FTIR) spectroscopy]. Swelling agents appeared between the clay layers in two ways: adsorbed and chemically bonded (Fig. 1). The amount of organic compound in the clays is listed in Table I from both the TGA and microanalysis results. The intercalated organic molecule was oriented along a specific direction in the intermolecular space because of the competition of various energy terms. The length of the organic chain determined the structure of the modified clay. The clay layers were expanded because of the appearance of the swelling agents for both K10 and KSF (XRD), which caused a disordered structure in the clays.

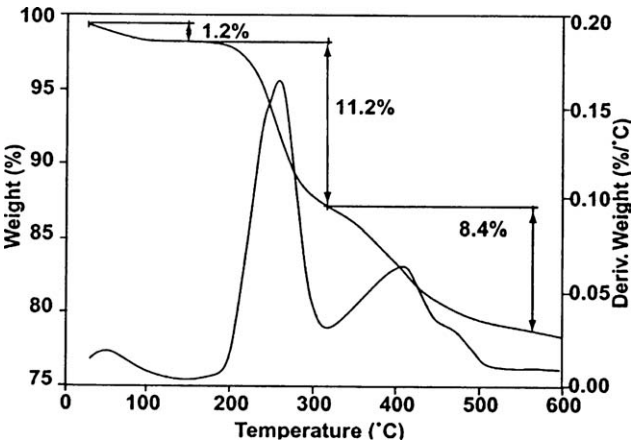

Figure 1 Weight loss and derivative weight loss versus the temperature for K10–C16 from TGA–DTG.

More details are given in the Supporting Information. The mechanism of interaction between the clays and swelling agents is illustrated in Figure 2. With a short carbon chain [Fig. 2(a)], the surfactant molecules are inserted between the clay layer in a parallel fashion. A tilting angle was postulated with longer chains, which increased with the alkyl chain length [Fig. 2(b)]. The chains were perpendicular from the clay surface layer because of the increasing chain length and van der Waals interactions between adjacent alkyl chains [Fig. 2(c)].

Ionomer–clay NCs

Structural evaluation by FTIR spectroscopy

The strength of interaction or attachment of the ionomer–clay NCs was examined with PA–FTIR spectroscopy. Figure 3 shows the spectra of PI and PI–K10 without and with clay modification. The bands between 2800 and 3000 cm^{-1} were related to the symmetric and asymmetric stretching modes of the —CH_2— and —CH_3 groups, respectively, in the cationic modifier and the ionomer. These bands did not shift with the addition of the unmodified or modified clays. The band at 1700 cm^{-1} was the C=O stretching mode from the hydrogen-bonded —COOH group of the ionomer. This peak position did not change after the addition of the clays; this indicated that no hydrogen bonds were formed between the carboxylic groups and the hydroxyl groups of the clays. The band at 1000–1200 cm^{-1}, ascribed to the Si—O—Si groups, appeared in all of the ionomer–clay samples. The FTIR spectra of the PI–KSF samples showed a similar trend. The structure of the ionomer–clay NCs was not affected by clay modification or the carbon number of the swelling agent. No new groups formed nor was a peak shift observed when the clay was mixed with PI. The solid-state ^{13}C-NMR spectra of PI–K10–C16 and PI–KSF–C16 (not shown) were quite similar; this indicated that there was no effect of the type of clay on the structure of the NCs.

Thermal stability

TGA was used to determine the thermal stability of the sample and the proportion of silicate in the material.[45] Table II summarizes the maximum decomposition temperature of the PI and PI–clay NC samples from the differential thermogravimetry (DTG) plots. The results show that the maximum decomposition temperature increased (458 to 466°C) with the addition of 10 wt % clay; this indicated a higher thermal stability of the NC. Frischer et al.[46] explained that the clay nanolayers acted as barriers to prevent volatile decomposition products from escaping the material. The ability to improve the thermal stability of a polymer with clay is due to its layered structure. The decomposition temperature of PI–K10–C12 was lower than those of the other NCs. This was due to the decomposition of C12. Other researchers[47,48] observed that the existence of swelling agents reduced the thermal stability of the polymers because of the decomposition of the swelling agents. In this study, a strong shoulder appeared before the main decomposition peak in the PI–K10–C12 curve, and a small shoulder was present in the

TABLE I
TGA and Microanalysis Results for the Modified Clays

	Swelling agent from TGA–DTG (wt %)			Microanalysis (wt %)	
Sample	Bound[b]	Unbound[c]	Total amount	Calculated from % of C	Calculated from % of N
K10–C12	6.7	—	6.7	7.6	3.2
K10–C16	8.4	11.2	19.4	20.1	12.7
K10–C18	3.0	14.9	17.8	23.6	16.7
KSF–C12		11.0[a]	11.0	12.3	9.6
KSF–C16	13.6	7.1	20.7	22.4	18.7
KSF–C18	15.8	12.9	28.6	29.5	23.5

[a] One broad peak was observed from 180 to 500°C.
[b] Refers to chemisorbed materials.
[c] Refers to physisorbed materials.

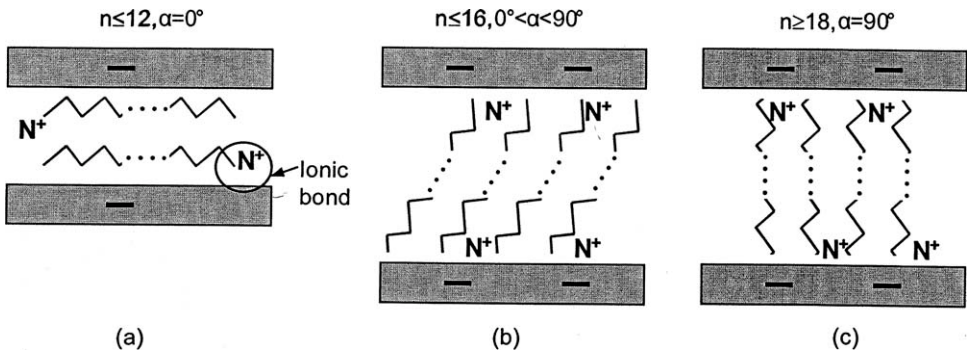

Figure 2 Mechanism of the interaction between the clays and swelling agents (n = number of carbons in each molecule, α = tilt angle).

PI–K10–C16 curve. This was due to the decomposition of the chemically adsorbed C12 and C16 modifiers, respectively. The TGA results show that the thermal stability of the ionomer was affected by the alkyl chain length of the swelling agents. The swelling agents with longer organic chains led to better thermal properties in the ionomer. The layered structure of clay offered a barrier effect to the evaporation of degraded molecules. The residue from TGA was mainly silica and metal oxide. The amount of residue from TGA (not shown) followed the order: PI–K10 > PI–K10–C12 > PI–K10–C16 > PI–K10–C18. This further indicated that the total amount of the swelling agent in the clay increased with the length of organic chain (Table I). The PI–KSF NCs showed a similar trend in thermal properties to the PI–K10 NCs. As shown in Table II, the decomposition temperature of the PI–KSF–C12 sample was lower than that of PI–K10–C12. This was because the dispersion and adhesion of KSF–C12 to PI was not the same as that of PI–K10–C12 due to the differences in their size and surface activity. However, a small difference was observed in the thermal stability of the PI–KSF and PI–K10 samples with C18 and C16 modification. This indicated that the long chain was necessary to prepare thermally stable organophilic MMT and, hence, NCs when the clay particle size was large.

Phase behavior

DSC measurements were carried out on the NC samples to investigate their thermal characteristics and transitions. Figure 4 shows the heat flow versus temperature curves of the ionomer and its NCs with modified K10 and KSF from the second run. We mentioned that PI had two transitions during heating: a cluster transition ($\sim$ 50°C) and PE melting ($\sim$ 95°C).[49] It was obvious that the cluster transition peaks of all of the NC samples became broad and shifted to lower temperature. This indicated that some reorganization took place in the cluster. Layered silica or intercalated clay layers with nanoscale sizes could insert into the cluster. The hydrophobicity of the organophilic MMT increased after modification.[50] However, a part of the clay surface may have remained compatible with the ionic domains. The PE melting temperature in the NC samples did not change compared to PI; this indicated that the PE chains were not disturbed by the presence of clay. However, the total heat flow calculated from the PE melting endotherm of the NCs showed a difference from that of PI. This was due to the crystalline nature of the clay and that of the organic swelling agent. In addition, clay fillers of different nature may differ in the strength of their adsorption of macromolecules. A clay with small particle size can act well as the core or center of a spherulite. However, those with particle sizes larger than the spherulitic core cannot form the center of a spherulite. The size of the clay particle, thus, influences the size distribution of crystals and, hence, the melting behavior. The low-temperature peak of the ionomer, which corresponded to the order–disorder transition temperature, shifted to a lower temperature with organic modification (Fig. 4). The negative shift in the

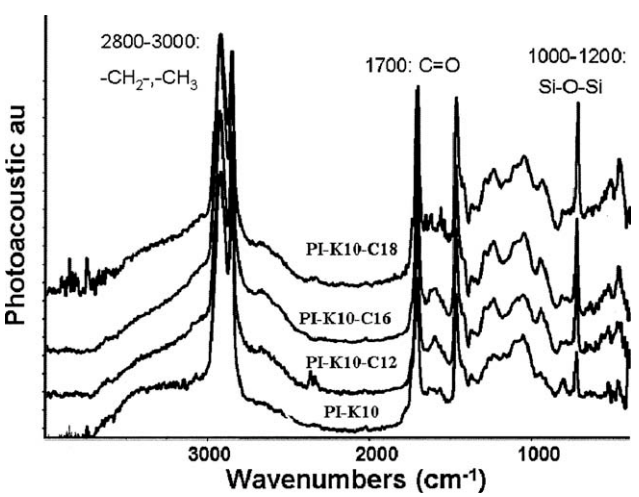

Figure 3 FTIR spectra of PI and PI–K10 NCs with or without clay modification.

TABLE II
TGA, MDSC, and XRD Results for PI and Its NCs

Sample	RHF (J/g)	NHF (J/g)	HF (J/g)	Crystallinity (%)		T_{max} from TGA (°C)
				MDSC	XRD	
PI	12.1	52.6	64.7	22.3	24.0	458.0
PI–K10	5.7	69.6	75.3	26.0	—	469.9
PI–K10–C12	19.0	88.7	107.7	37.1	32.1	466.2
PI–K10–C16	21.6	84.7	106.2	36.6	38.3	470.9
PI–K10–C18	24.4	86.4	110.8	38.2	28.2	470.0
PI–KSF	2.5	73.7	76.3	26.3	—	468.4
PI–KSF–C12	17.8	89.8	107.5	37.1	35.4	463.3
PI–KSF–C16	20.6	87.0	107.6	37.1	34.9	469.0
PI–KSF–C18	29.5	70.9	100.4	34.6	32.1	471.9

T_{max} = maximum decomposition temperature; RHF = reversing heat flow; NHF = nonreversing heat flow; HF = total heat flow.

order–disorder transition indicated a plasticization effect of the ionomer clusters by the long alkyl chain modification.

MDSC was used to monitor the effect of the addition of the clays and clay modification on the PE crystal morphology. The transition behavior of PI from the MDSC study was reported in our earlier article, which included total heat flow (HF), reversing (RHF), and nonreversing heat flows (NHF).[49] Table II lists the total, reversing, and nonreversing heat flows and the crystallinity of PI and its NCs at a 0.5°C/min cooling rate. Interestingly, although the reversing heat flow component was smaller in PI–K10 and PI–KSF than in PI, it increased with the chain length of the swelling agent. This was because the long-chain crystal structure acted as a nuclei during the PE crystallization and contributed to the total crystallinity. The crystal structure of PE in the ionomer was more ordered. The reversing component of the total heat flow directly related to the entanglement density of the linear polymer melt. The previous results indicated that the clay modification affected the crystallization behavior and, hence, melting of PE in the NC. It is well known that fillers influence the crystallization and melting behavior of a polymer by reducing its mobility, which results from polymer–filler interaction. Thus, the clay played a major role, not only acting as a nucleating agent for the crystallization process but also affecting the transfer of the polymer across the melt–crystal interface, that is, the growth process. The reversing heat flow was similar between K10 and KSF when the same swelling agent was used; this indicated that the swelling agent affected the formation of linear crystals rather than the clay particle size. Compared to the ionomer, the nonreversing heat flow of all of the NC samples was higher. The addition of the clay reduced the regularity of the PE crystal in the ionomer. The nonreversing heat flow in the K10 systems was affected by the clay modification, whereas it did not change with different swelling agents. However, the type of swelling agent affected the crystal morphology in the KSF systems. PI–KSF–C18 exhibited the lowest value of nonreversing heat flow. The total heat flow of the ionomer increased with the addition of either K10 or KSF, especially when the modified clays were used. This was due to the crystal structure of the clays and the existence of the swelling agent. However, the total heat flow did not change with the chain length of the swelling agents. These results demonstrate that the crystallinity of the ionomer was affected by the clay modification. The crystallinity of PI–K10 or PI–KSF was higher than that of PI because of the crystalline nature of the clays. The way that the clay affected or reduced the crystallization behavior followed the following order: PI < PI–K10 < PI–KSF.

The crystallization behavior of the ionomer was affected by the swelling agent and the type of clay. Figure 5 shows the crystallization curves of the

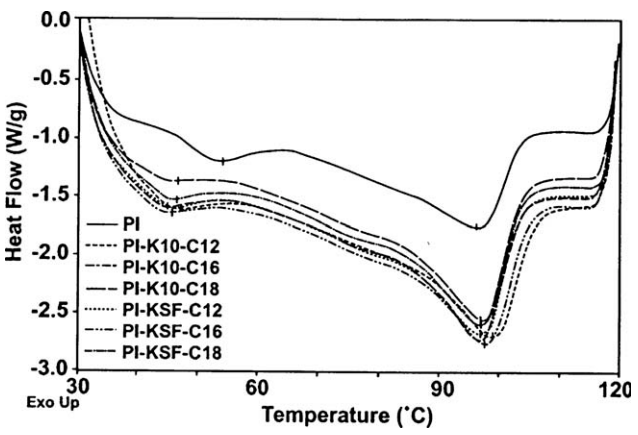

Figure 4 Heat flow versus the temperature for PI and its composites with K10 and KSF from DSC.

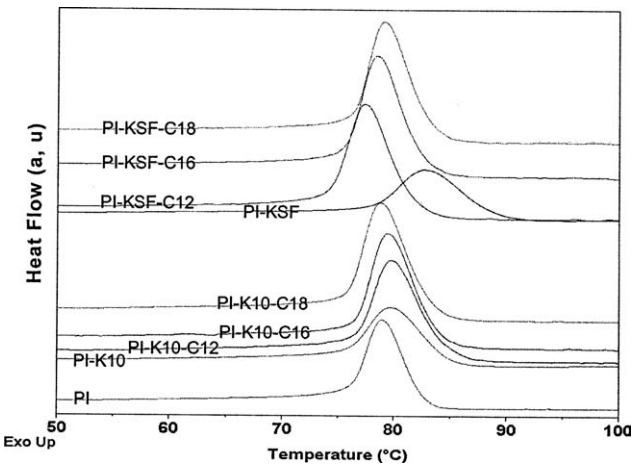

Figure 5 Crystallization behavior of the ionomer with the clays as a function of temperature at a 2°C/min cooling rate.

ionomer with various clays. In all the cases, an exothermic peak was observed during cooling, which was due to PE crystallization. However, the maximum crystallization temperature and the enthalpy in each sample varied. PI had the lowest enthalpy and, thus, the lowest crystallinity. The peak became broader with the addition of the clays; this indicated that the crystallization process took longer. The entropy of crystallization (ΔS_c) was calculated with the enthalpy of crystallization (ΔH_c) and the crystallization temperature (T_c) with the following relation:

$$\Delta S_c = \Delta H_c / T_c$$

In the K10 systems, the crystallization temperature of the ionomer changed marginally with the swelling agent, but the enthalpy was higher with the modified clay than with the unmodified clay (Fig. 5). This indicated that K10 affected the crystallization of the ionomer more than did the swelling agents. The increase in the enthalpy indicated an increase in the crystallinity. However, the crystallization temperature was different in the KSF systems. PI–KSF had the highest crystallization temperature; this indicated that KSF promoted the crystallization earlier. The crystallization temperature decreased with the addition of the swelling agents in the KSF systems but increased with increasing chain length of the swelling agent. The enthalpy and entropy of the crystallization were more or less similar between the K10 and KSF systems.

Morphology study

XRD is the most commonly used tool to measure the *d*-spacing change for polymer–clay NCs to probe and illustrate the structure and morphology of the NCs. The crystallinity and morphology of the ionomeric hybrids were evaluated from an XRD study. Figure 6 shows the XRD patterns of PI–K10–C*x* (x = 0, 12, 16, or 18). It was clear that there was a sharp peak at about 20° with two halos on the left and right sides, respectively. This sharp peak was due to the crystalline nature of PE in PI, and the halos were related to the amorphous phase of PE.[49] Figure 6 shows that the sharp peak did not shift with the addition of the clays. This observation indicated that the *d*-spacing of the PE crystal did not change. The crystallinity was obtained from the peak area with a peak-fitting program. The PI–KSF–C*x* (x = 0, 12, 16, or 18) NCs showed the same trend. The crystallinity of each sample is listed in Table II. The XRD results were in line with the MDSC results and showed that unmodified/modified clay increased the crystallinity of the ionomer, but the melting point did not change.

The morphology of NCs and the gallery height of the clay will change if there is a strong interaction between the modified clay and the polymer. As shown clearly (Fig. 6), there was no noticeable diffraction peak in the curves in the region 0–10°; this indicated that the clay structure was either completely broken down, or it led to a partially disordered house-of-cards structure. The disappearance of a peak in this region confirmed the exfoliated structure of the silicate layer in the ionomer matrix after solution blending.[8,42] In general, the clay structure in this study was characterized by the coexistence of exfoliated and random layers. The mixed exfoliated/disordered structure, intrinsic to MMT, resulted in a chemical and size heterogeneity of the MMT layer. The further layer expansion capacity of the organoclay by the ionomer was then determined by the thermodynamic balance of the compatibility of the modified clay and the ionomer and also by the viscosity of the ionomer. Although the ionomer and clay were both hydrophilic and exhibited good

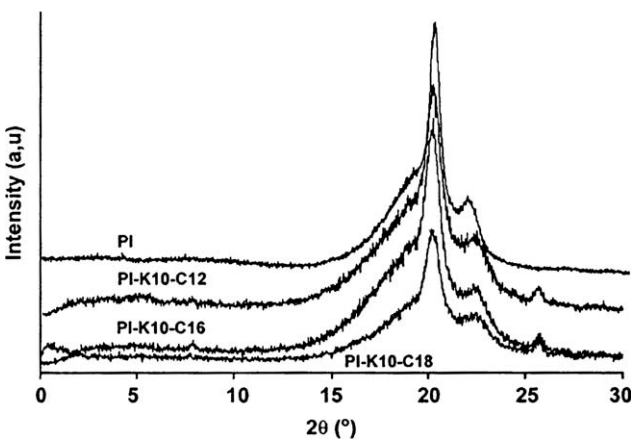

Figure 6 Overlaid XRD patterns of PI–K10–C*x* (x = 0, 12, 16, or 18).

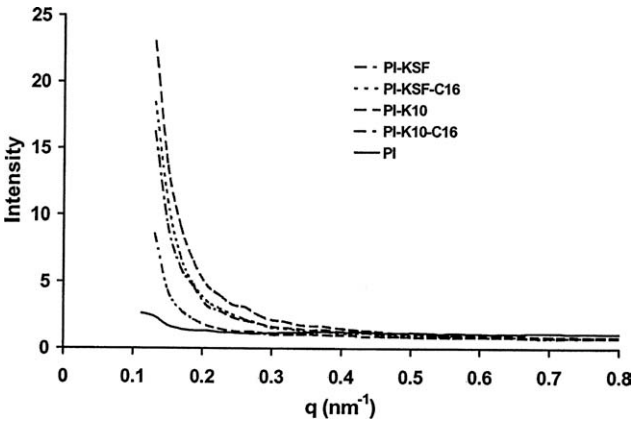

Figure 7 SANS profiles of PI with various clays.

compatibility between each other without modification, some hydrogen bonding interaction could not be ruled out with the ionomer and clay. In the C18-modified system, the interaction between the organophilic clay and the PE part occurred because of the integration of the long alkyl chain with the backbone and, hence, a capillary channel of the latter in the clay tactoids. This situation could also result in complete exfoliation. The *d*-spacing of K10–C18 was high enough to further intercalate part of the matrix chains. The compatibility of the ionomer and clay or interaction between C18 incorporated in the organoclay and the PE phase played a dominant role in determining the diffusion behavior and the extent of further intercalation/exfoliation.

The SANS technique demonstrates the morphology of polymer crystals and ionic domains. Figure 7 shows the SANS plots of the ionomer and its NCs with the unmodified/modified clays. In all cases, an upturn decreased with increasing q, which was related to the ionic domains. The upturn shifted with the addition of the clay from $q = 0.11$ nm^{-1} (PI $d = 57$ nm) to $q = 0.13$ nm^{-1} (NC $d = 49$ nm). The intensity of the peak varied for different samples. The NCs showed a much higher peak intensity than PI; this indicated the presence of a larger number of scattering sites. The effect of clay modification on the ionic groups was different in the K10 and KSF systems. The PI–K10 curve showed a higher intensity than that of PI–K10–C16; this indicated that the miscibility of K10 in the ionomer was improved after the clay modification. The phase separation was reduced with modified K10. However, the results in the KSF systems did not follow this trend. The peak intensity of PI–KSF was much lower than that of PI–KSF–C16. This indicated that the miscibility was not improved after the clay modification. The intensity of the upturn in PI–K10 was higher than that of PI–KSF. However, the upturn of PI–K10–C16 was lower than that of PI–KSF–C16; this indicated that the dispersion of the clay in the ionomer was more homogeneous with modified K10 than with modified KSF. The clay modification improved the miscibility between the clay and the ionomer only when the clay size was small.

AFM, with its high resolution, allows visualization of the morphology, mapping distribution, and nanostructure in a material or hybrid. AFM measurement was done on the samples to investigate the distribution of the clay in the polymer. Figure 8 shows the

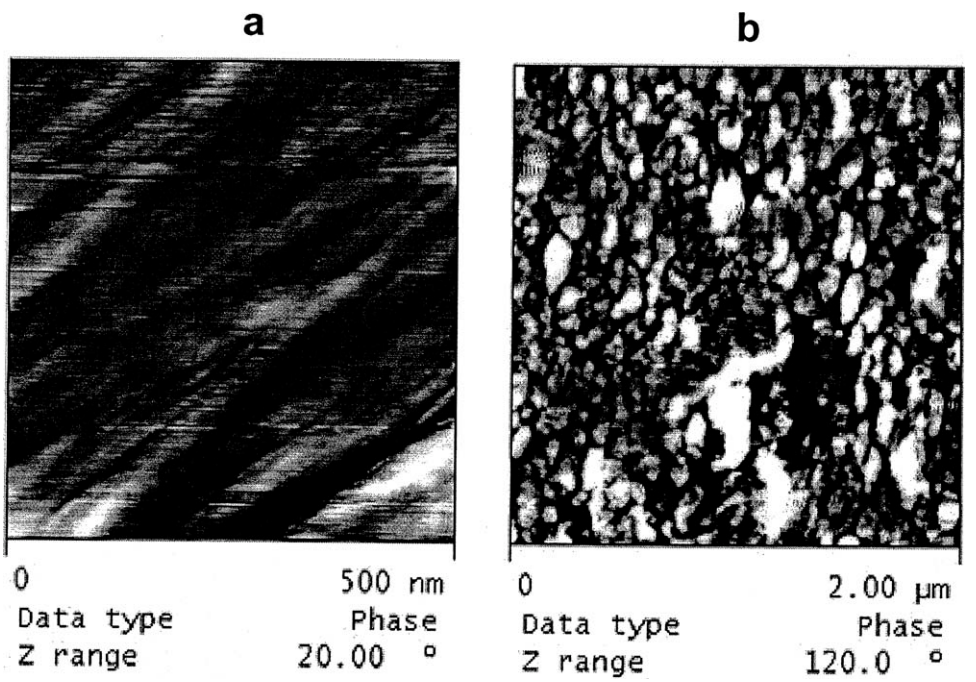

Figure 8 AFM images of (a) PI–K10–C18 and (b) PI–KSF–C16.

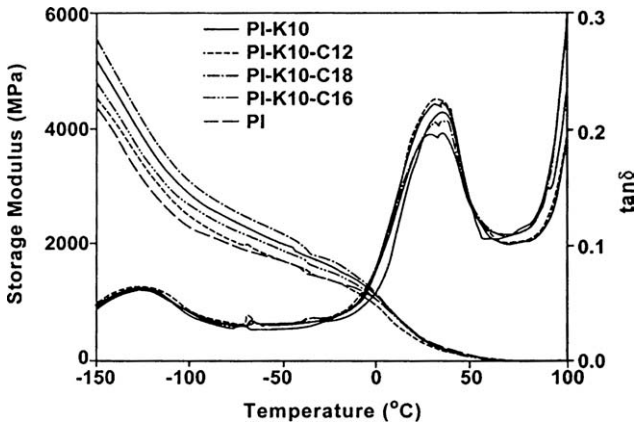

Figure 9 Storage modulus and tan δ versus the temperature for PI and PI–K10–Cx (x = 0, 12, 16, or 18) from DMA.

phase images of PI–K10–C18 and PI–KSF–C16 as measured on the NC surface. Hard tapping on the sample surface was needed to get better contrast between the two phases (the dark and light phases were due to the clay and the ionomer, respectively). Figure 8(a) shows the layered structure of clay in the polymer matrix of PI–K10–C18. A parallel arrangement of the layers was retained with nanoseparation. The distance between the sheets appeared to be about 25 nm. Figure 8(b) shows the granular morphology of the crystalline sample PI–KSF–C16. In PI–KSF–C16, the modified clay aggregated to some extent and dispersed in the polymer matrix. The aggregated clay size remained at the nanoscale.

Dynamic mechanical properties

The dynamic mechanical properties of the NCs were evaluated with temperature. Figure 9 shows the storage modulus and tan δ plots versus temperature of PI and PI–K10–Cx (x = 0, 12, 16, or 18). The NCs exhibited a higher storage modulus compared to PI. In the NCs with modified clay, the storage modulus increased with increasing length of carbon chains, especially in PI–K10–C18, where the increase was more than 25%. The segmental motion near the organic–inorganic interface was restricted because of improved adhesion between the ionomer and the clay, so the storage modulus increased. The hydrophilicity of the clay decreased with increasing carbon number of the surfactant, and hence, the compatibility with the PE part of the ionomer increased. The restriction of polymer chain motion was in direct proportion to the length of the carbon chain of the swelling agents. Interestingly, PI–K10 without modification showed a higher compatibility with the ionomer. Its storage modulus was lower than PI–K10–C18 but higher than the others. If clay was modified by a swelling agent, the phase separation behavior between the PE part of the ionomer matrix and clay was improved. However, the miscibility between ionic groups and clay remained better with unmodified clay because of its hydrophilic nature. The storage modulus decreased with increasing temperature in all of the samples. The storage modulus of the NC samples was higher than that of PI. Also, the storage modulus of the C18-modified NCs was higher than the C12/C16 NCs. Such a reinforcing effect was the result of better dispersion of silicate layers in this exfoliated NC. It was evident that, among the three organoclay (C12, C16, and C18) hybrids, C12 had the lowest degree of exfoliation and, hence, a lower dispersion. Thus, shorter alkyl ammonium ions in the gallery restricted intragallery diffusion.

The tan δ peak position demonstrates the cluster transition behavior of hybrids. The change in the transitions reflects a morphological change in the materials. As reported,[51] the transitions of PI at −130°C was due to the γ transition of the PE crankshaft rotation transition, and the one at about 32°C was related to the ionic phase transition. In Figure 9, the tan δ curve shows two significant transition peaks: −130 and about 32°C. The transition at −130°C did not change with the addition of clay. The peak at about 32°C for all of the NCs shifted to a slightly higher temperature compared to PI, which meant that the motion of ionic groups in the cluster was restricted. The clay layers resided in the cluster and possibly remained persistent in this case. Entropy decreased because of the confinement of C12 within the gallery, but the enthalpy interaction between the ionomer and C12 favored mixing and its solubilization. The ionic transition peak became broad as a result of the reorganization of the cluster that took place by the addition of the clay and because of coulombic interaction.

Figure 10 shows the DMA results of the PI and PI–KSF–Cx (x = 0, 12, 16, or 18) samples. The improvement of the storage modulus was also seen in all of the PI–KSF NCs. The storage modulus of PI–KSF was lower than those of PI–KSF–C16 and

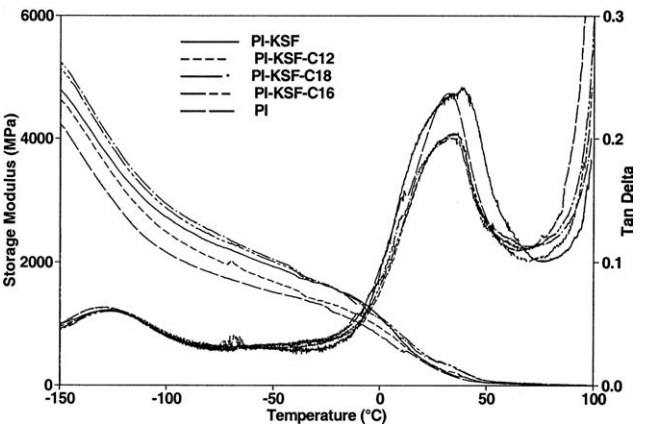

Figure 10 DMA results for PI and PI–KSF–Cx NCs (x = 0, 12, 16, or 18).

PI–KSF–C18 and similar to that of PI–KSF–C12. This was because KSF had a bigger particle size and lower surface area than K10. This affected the adhesion between the ionomer and KSF. The phase separation was more prominent in PI–KSF than PI–K10. The tan δ value of PI–KSF was slightly lower than PI. Thus, it was clear that clay could improve the mechanical properties of the ionomer. The improvement in the storage modulus depended on both the carbon chain length of the swelling agents and the nature of the clay.

CONCLUSIONS

The interfacial interaction between ionomer and clays was varied with swelling agents of different chain lengths. MMT (K10 and KSF), with its unique structure, was chosen to prepare ionomer–clay NCs. To improve the miscibility between the ionomer and the clay, clay modification was carried out with various swelling agents. The organic chains inserted into the clay gallery, both physically adsorbed and chemically bonded (XRD and TGA), and the formation of links between organic chains and the clays were affected by the surfactants.

PI–clay NCs were prepared with the modified and unmodified clays. The PA–FTIR spectra showed that there was no bonded coordination between PI and the modified/unmodified clays, which indicated that the structure of the NCs was not affected by the swelling agents and the type of clay. XRD and AFM studies revealed that a partly exfoliated NC was formed, whereas the stacking of several silicate layers on a nanoscale existed in the ionomer. The storage modulus increased dramatically, especially with the C18 surfactant, but the difference in storage modulus with different clays was marginal. The ionic transition temperature shifted to a higher temperature in all of the NCs, which indicated that part of the clay existed in the ionic cluster. The DSC results show the insertion of the clay in the cluster due to the shifting of the cluster transition peak. MDSC and XRD results reveal that the crystallinity of the NCs was higher than the ionomer because of the swelling agents and also because of the crystalline nature of the clay. The relative level of interaction between the polymers, the organic modifier, and the silicate layer played an important role in determining the properties of the NCs.

References

1. Lakshminarayanan, S.; Lin, B.; Gelves, G. A.; Sundararaj, U. J Appl Polym Sci 2009, 112, 3597.
2. Palza, H.; Vergara, R.; Yazdani-Pedram, M.; Quijada, R. J Appl Polym Sci 2009, 112, 1278.
3. Nguyen, Q. T.; Baird, D. G. Adv Polym Technol 2006, 25, 270.
4. Wu, T.; Liu, A.; Xie, T.; Yang, G. J Appl Polym Sci 2008, 110, 2727.
5. Pinnavaia, T. J.; Beall, G. W. Polymer–Clay Nanocomposites; Wiley: Chichester, United Kingdom, 2000.
6. Bhiwankar, N. N.; Weiss, R. A. Polymer 2006, 47, 6684.
7. Tamura, K.; Yokoyama, S.; Pascua, C. S.; Yamada, H. Chem Mater 2008, 20, 2242.
8. Velmurugan, R.; Mohan, T. P. J Mater Sci 2004, 39, 7333.
9. Naka, K.; Chujo, Y. Chem Mater 2001, 13, 3245.
10. Blackwell, R. I.; Mautitz, K. A. Polymer 2004, 45, 3457.
11. Brinker, C. J.; Scherer, G. W. Sol–Gel Science: The Physics and Chemistry of Sol–Gel Processing; Academic: San Diego, California, 1990.
12. Greesh, N.; Hartmann, P. C.; Sanderson, R. D. Macromol Mater Eng 2009, 294, 206.
13. Patino-Soto, A. P.; Sanchez-Valdes, S.; Ramos-Devalle, L. F. J Polym Sci Part B: Polym Phys 2008, 46, 190.
14. Ogawa, M.; Tsujimura, M.; Kuroda, K. Langmuir 2000, 16, 4206.
15. Nakas, G. I.; Kaynak, C. Polym Compos 2009, 30, 357.
16. Costache, M. C.; Heidecker, M. J.; Manias, E.; Wilkie, C. A. Polym Adv Technol 2006, 17, 764.
17. Kelarakis, A.; Giannelis, E. P.; Yoon, K. Polymer 2007, 48, 7567.
18. Kurose, T.; Yudin, V. E.; Otaigbe, J. U.; Svetlichnyi, V. M. Polymer 2007, 48, 7130.
19. Kurian, M.; Dasgupta, A.; Beyer, F.; Galvin, M. E. J Polym Sci Part B: Polym Phys 2004, 42, 4075.
20. Wu, D.; Zhou, C.; Zhang, M. J Appl Polym Sci 2006, 102, 3628.
21. Gao, Q. M.; Giraldo, O.; Tong, W.; Suib, S. L. Chem Mater 2001, 13, 778.
22. Joshi, M.; Viswanathan, V. J Appl Polym Sci 2006, 102, 2164.
23. Rong, J. F.; Jing, Z. H.; Li, H. Q.; Sheng, M. Macromol Rapid Commun 2001, 22, 329.
24. Sikdar, D.; Katti, D. R.; Katti, K. S. J Appl Polym Sci 2008, 107, 3137.
25. Tiwari, R. R.; Natarajan, U. J Appl Polym Sci 2008, 110, 2374.
26. Liu, T.; Tjiu, W. C.; Tong, Y.; He, C.; Goh, S. S. J Appl Polym Sci 2004, 94, 1236.
27. Sanjay, K.; Nayak, S. M. J Appl Polym Sci 2009, 112, 778.
28. Mohan, T. P.; Ramesh Kumar, M.; Velmurugan, R. J Mater Sci 2006, 41, 5915.
29. Zeng, C. C.; Lee, L. J. Macromolecules 2001, 34, 4098.
30. Bellucci, F.; Terenzi, A.; Leuteritz, A.; Pospiech, D.; Frache, A.; Traverso, G.; Camino, G. Polym Adv Technol 2008, 19, 547.
31. Kim, D. W.; Blumstein, A.; Tripathy, S. K. Chem Mater 2001, 13, 1916.
32. Rajkiran, R.; Tiwari, U. N. J Appl Polym Sci 2008, 110, 2374.
33. Yuan, X.; Li, C.; Guan, G.; Xiao, Y.; Zhang, D. J Appl Polym Sci 2008, 109, 4112.
34. Yano, K.; Usuki, A.; Okada, A. J Polym Sci Part A: Polym Chem 1997, 35, 2289.
35. Clarke, N.; Hutchings, L. R.; Robinson, I.; Elder, J. A.; Collins, S. A. J Appl Polym Sci 2009, 113, 1307.
36. Okamoto, M.; Morita, S.; Kim, Y. H.; Kotaka, T.; Tateyama, H. Polymer 2001, 42, 1201.
37. Chen, B.; Evans, J. R. G. Polymer 2008, 49, 5113.
38. Shen, L.; Phang, I. Y.; Liu, T.; Zeng, K. Polymer 2004, 45, 8221.
39. Ratna, D.; Divekar, S.; Samui, A. B.; Chakraborty, B. C.; Banthia, A. K. Polymer 2006, 47, 4068.
40. Zhang, W.; Li, M. K. S.; Yue, P. L.; Gao, P. Langmuir 2008, 24, 2663.
41. Song, M.-K.; Park, S.-B.; Kim, Y.-T.; Rhee, H.-W. Mol Cryst Liq Cryst 2003, 407, 411.

42. Parent, J. S.; Liskova, A.; Resendes, R. Polymer 2004, 45, 8091.
43. Kovarova, L.; Kalendova, A.; Malac, J.; Vaculik, J.; Malac, Z.; Simonik, J. Soc Plast Eng Annu Tech Conf 2002, 60, 2291.
44. Carter, C. M. Soc Plast Eng Annu Tech Conf 2001, 59, 3210.
45. Gao, Y.; Choudhury, N. R.; Dutta, N. J Polym Eng 2006, 26, 853.
46. Frischer, H. R.; Gielgens, L. H.; Koster, T. P. M. Acta Polym 1999, 50, 122.
47. Parija, S.; Nayak, S. K.; Verma, S. K.; Tripathy, S. S. Polym Compos 2004, 25, 646.
48. Wang, Z.; Pinnavaia, T. J. Chem Mater 1998, 10, 1820.
49. Gao, Y.; Choudhury, N. R.; Dutta, N.; Matisons, J.; Shanks, R.; Weiss, B. J. Therm Anal 2003, 73, 361.
50. Pheng, B. K. The Chemistry of Clay–Organic Reactions; Wiley: New York, 1974.
51. Gao, Y.; Choudhury, N. R.; Dutta, N.; Matisons, J.; Reading, M.; Delmotte, L. Chem Mater 2001, 13, 3644.